

Additive Manufacturing of Fatigue Resistant Materials: Avoiding the Early Life Crack Initiation Mechanisms during Fabrication

Jonathan Pegues^{1,2}, Michael Roach³, Nima Shamsaei^{1,2*}

¹Department of Mechanical Engineering, Auburn University, Auburn, AL

²National Center for Additive Manufacturing Excellence (NCAME), Auburn University,
Auburn, AL

³Department of Biomedical Materials Science, University of Mississippi Medical Center,
Jackson, MS

*Corresponding author:

Email: shamsaei@auburn.edu

Phone: (334) 844 4839

Abstract

The full potential of additive manufacturing (AM) has been limited by the process induced defects within the fabricated materials. Defects such as lack of fusions and gas entrapped pores act as stress concentrators and result in premature fatigue crack initiation, severely limiting the applicability of AM in fatigue-critical applications. However, by understanding the failure mechanisms associated with AM materials and leveraging the intimate localized thermal input (i.e. process conditions), the failure mechanisms for some materials may be avoided during the fabrication process. This study investigates the crack initiation behavior of an AM austenitic stainless steels subjected to fatigue testing. The microstructural features responsible for fatigue crack initiation are captured at the surface by ex-situ electron backscatter diffraction. Results show that the higher cooling rates during AM offer the opportunity to fabricate fatigue resistant austenitic stainless steel parts by avoiding the microstructural features that are most detrimental to fatigue performance.

Keywords: Laser powder bed fusion, Crack nucleation, Twin boundary, Heat treatment

Introduction

Adoption of additive manufacturing for fatigue critical applications has been plagued by the presence of process induced defects such as surface roughness and/or porosity. These defects introduce significant stress concentrations leading to early fatigue life crack initiation, which can significantly affect the fatigue behavior of additive manufactured parts. While most researchers have focused on optimizing the additive manufacturing process to achieve maximum density, the fabrication of defect free AM parts has not been realized.

Researchers have long suggested that establishing the feedstock-process-structure-property-performance (FPSPP) relationships could lead to the ability to additively manufacture more fatigue resistant materials [1]. The goal of applying this approach is to leverage the material and processes effects on the microstructure to tailor the material properties for a specific service condition and ultimately improve part performance. This type of approach is essentially application driven, tailoring of the microstructure and is accomplished through the intimate relationship between the supplied thermal history and the resulting microstructure. To date, however, this approach has been overshadowed by the effect of defects, which typically outweigh any improvements in microstructure [1-3].

Austenitic stainless steels are exceptionally tough alloys having moderate strength and high ductility. Unlike most engineering alloys, austenitic SSs are less susceptible to inclusions and porosity that typically plague the high cycle fatigue (HCF) behavior of common metallic materials [4, 5]. Inclusions and porosity, create stress concentrations that often lead to crack initiation and ultimately fatigue failure. For austenitic SSs, with exceptional toughness, can accommodate these types of stress concentrations without initiating early life fatigue cracks and are instead sensitive to microstructural features [4, 6].

Previous studies have revealed that annealing twin boundaries (Σ 3-TB) within the microstructure of 304L and 316L SSs are the most susceptible to crack initiation [4, 5, 7-9]. Specifically, Σ 3-TB that are oriented on the surface at approximately 45° from the loading direction are the most likely feature to initiate a dominant crack leading to failure. The deformation characteristics of these boundaries results in elastic incompatibilities near the boundary which lead to compliance stresses which can result in slip behavior near the boundary. As slip accumulates, persistent slip bands form resulting in intrusions/extrusions near the boundaries. These intrusions/extrusions are known to create micro-cracks that can develop into propagating cracks not only at Σ 3-TB but high angle grain boundaries (HAGB) as well [4]. This same crack initiation behavior can be exacerbated under increasingly greater loads which can create plastic incompatibilities in conjunction with the elastic ones leading to much faster crack formation.

It was suggested previously that the ability to control the Σ 3-TB/HAGB orientations or density during fabrication could lead to improved fatigue resistance [4], however, the means to control these specific boundaries was not known at the time. The emergence of additive manufacturing as an advanced manufacturing technique, however, has supplied the catalyst to manufacture austenitic stainless steel with limited Σ 3-TB/HAGB. In this study, the fatigue behavior of laser beam powder bed fusion (LB-PBF) austenitic stainless steels is investigated. These stainless steel alloys may provide early insight into how the FPSPP relationships can be

leveraged to fabricate more fatigue resistant materials by avoiding the typical failure mechanisms responsible for crack initiation.

Experimental Methods

Rectangular 304L SS specimen blanks were fabricated horizontally on an EOS M290 using standard 316L stainless steel process parameters. Specimens were stress relieved at 400°C for 1 hr and furnace cooled before being removed from the substrate. The blocks were then machined into standard cylindrical dogbone fatigue (CDF) specimens and non-standard square gage fatigue (SGF) specimens as shown in Figure 1. A set of specimens from each alloy was solution annealed at 1050°C for 1 hr then water quenched. All specimens were longitudinally polished to a mirror finish using silicon carbide grinding papers then further electro-polished using Struers A2 solution to obtain a pristine surface for EBSD analysis.

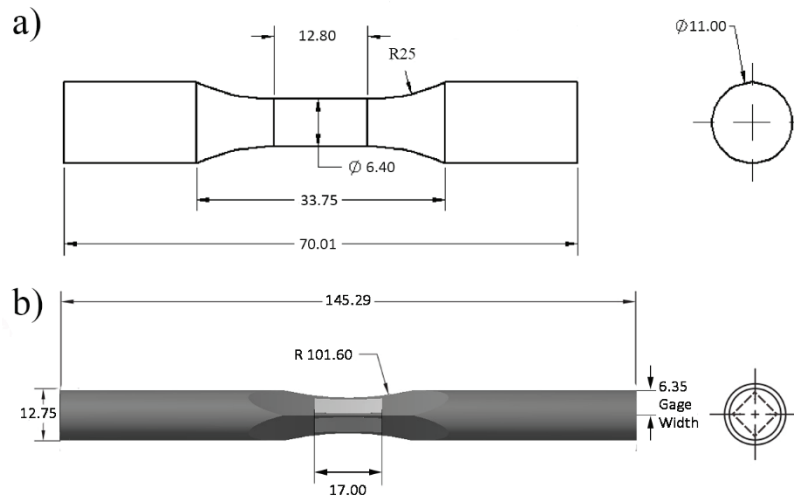


Figure 1: Specimen geometry for (a) cylindrical dogbone and (b) square gage fatigue specimens.

Microstructural characterization was carried out on a Zeiss FE-SEM using an EDAX electron backscatter diffraction (EBSD) detector and OIM software. Analysis was performed on each surface. Surfaces whose normal is perpendicular to the build direction are defined as ZXY and surfaces with normal is parallel with the building direction are defined as YXZ per ASTM WK49949 [10]. These directions, in relation to the specimen, are shown in Figure 2. All fatigue tests were conducted on an MTS servo-hydraulic test frame with 100 kN capacity. The CDF specimens were tested at several stress amplitudes until complete failure while the SGF specimens were tested at a single stress amplitude and interrupted starting at 10% of their expected life to failure to observe crack initiation. During the interrupted periods the specimens were loaded into the SEM and micro cracks were located and mapped using EBSD. A constant loading rate was used for all fatigue testing to avoid any load rate effects for these materials.

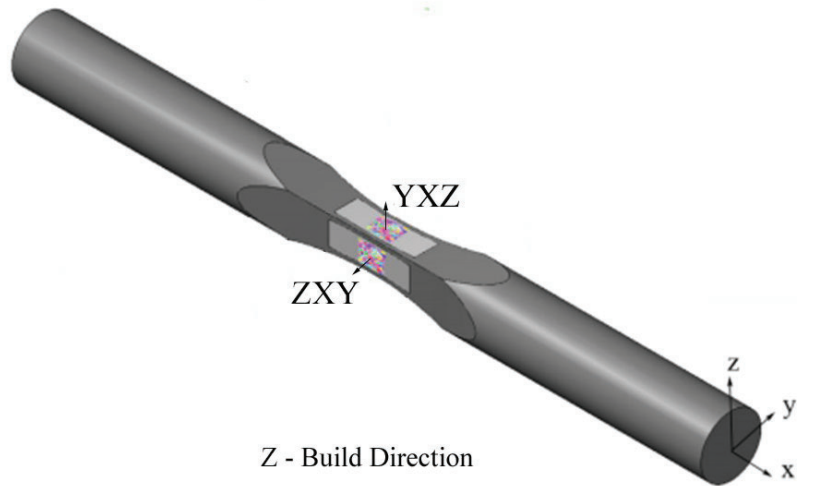


Figure 2: Orientation and directions for the square gage fatigue specimens.

Experimental Results

Microstructure

The microstructural characteristics for both (a) 304L SS stress relieved (304L-SR) and (b) 304L SS solution annealed (304L-SA) conditions are similar and are shown in Figure 3. On the left is the inverse pole figure (IPF) plot with the corresponding grain boundary misorientation chart and pole figure to the right. There are some remarkable characteristics for both alloys including a $\langle 011 \rangle$ texture, low density of HAGBs, and no easily-identifiable $\Sigma 3$ -TB. The $\langle 011 \rangle$ texture, which is approximately 4X the random, occurs due to the $\langle 001 \rangle$ easy growth direction and the fast moving heat source. Sun et al. [11] showed that scanning strategy can result in various melt pool geometries with shallow melt pools showing a $\langle 001 \rangle$ texture and deeper melt pools resulting in the $\langle 011 \rangle$ texture observed in this study. It should be noted, however, the texture is not perfectly aligned with the machined surface of the specimen as indicated by the 011 pole figure being slightly rotated about A2.

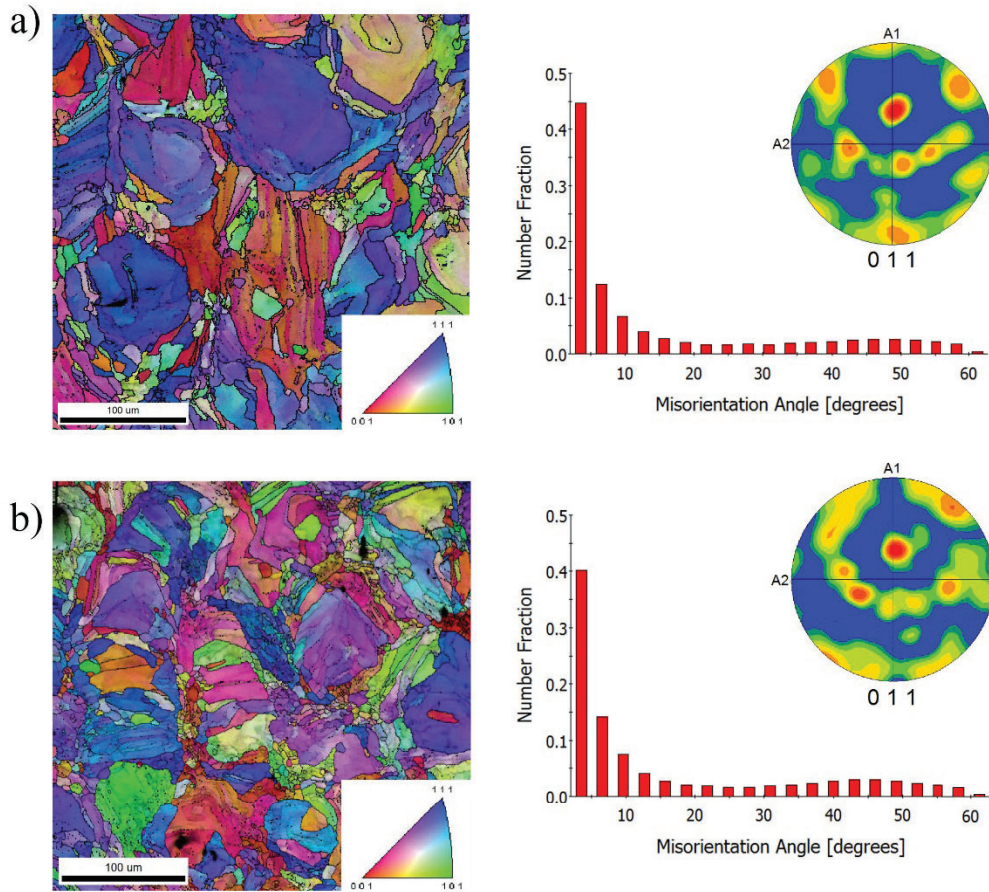


Figure 3: Inverse pole figure plot with grain boundary misorientation plots and pole figures for (a) 304L-SR and (b) 304L-SA conditions.

The grain morphology for YXZ and ZXY surfaces were observably different for both 304L-SR and 304L-SA specimens as shown in Figure 4. The ZXY surfaces grains were slightly elongated in the build direction where the YXZ grains were mostly equiaxed in its plane. Table 2 shows the average grain diameters and standard deviations for both surfaces and for both thermal treatment condition. Due to the elongated grains in the build direction, the ZXY surfaces had larger average grain diameters and standard deviations than the YXZ surfaces. The 304L-SA specimens showed a roughly 12% increase in grain size for both YXZ and ZXY surfaces. The differences in grain sizes for each surface, though small, can result in different deformation behaviors for each surface. For instance, larger grains typically show higher slip activity than smaller grains which can have significant implications on the crack initiation behavior as it is typically dominated by dislocation activity at the surface [12, 13].

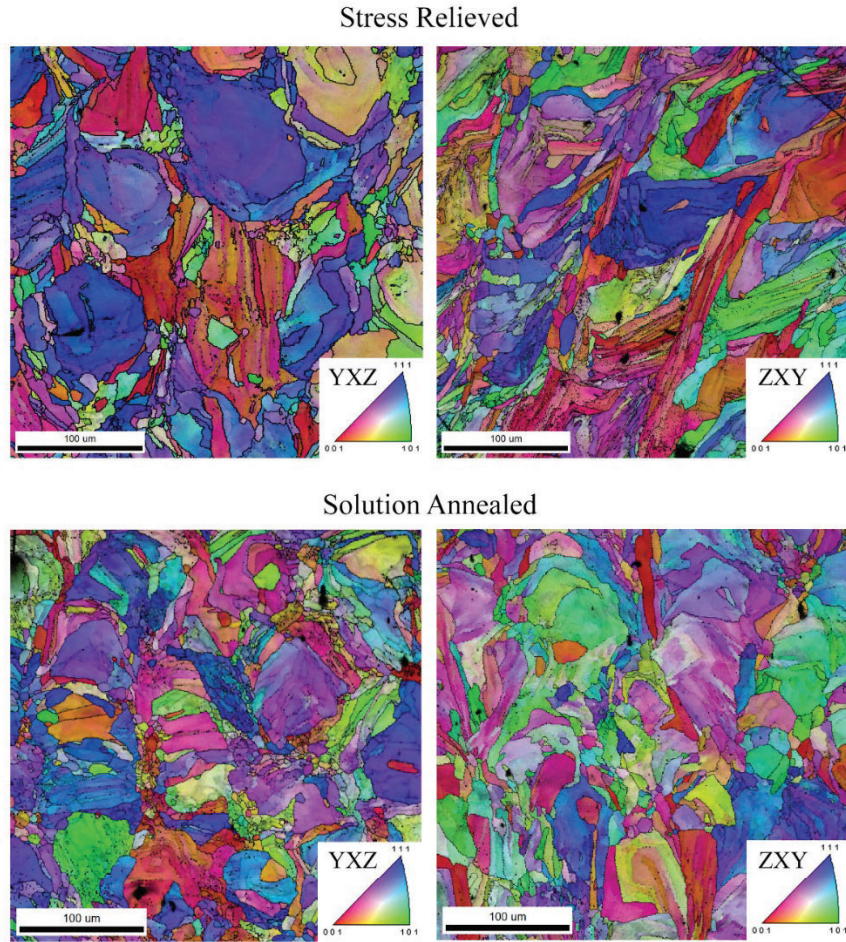


Figure 4: Micrographs for 304L-SR (top) and 304L-SA (bottom) showing grain structure for YXZ surfaces (left) and ZXY surfaces (right).

Table 1: Grain sizes for 304L-SR and 304L-SA for both YXZ and ZXY surfaces.

Surface	Grain Size (μm)	Standard Deviation (μm)
Stress Relief – 400°C 1-hr, furnace cooled		
YXZ	11.94	8.75
ZXY	13.28	10.12
Solution Anneal – 1050°C 1-hr, water quench		
YXZ	13.44	10.48
ZXY	14.75	12.13

Fatigue Behavior

The fatigue results, surprisingly, show improved fatigue resistance for the 304L-SR condition compared to wrought 304L stainless steel. Figure 5 shows the stress-life fatigue results and corresponding Basquin curves. The 304L-SR condition showed an increase in fatigue life one to two orders of magnitude for a given stress amplitude. This improved fatigue resistance is surprising for LB-PBF material, especially in the high cycle fatigue (HCF) regime which is often dominated by crack initiation at defects. The majority of the HCF life is often spent in the crack initiation stage which suggest that the improved fatigue resistance is a result of improved resistance to crack initiation.

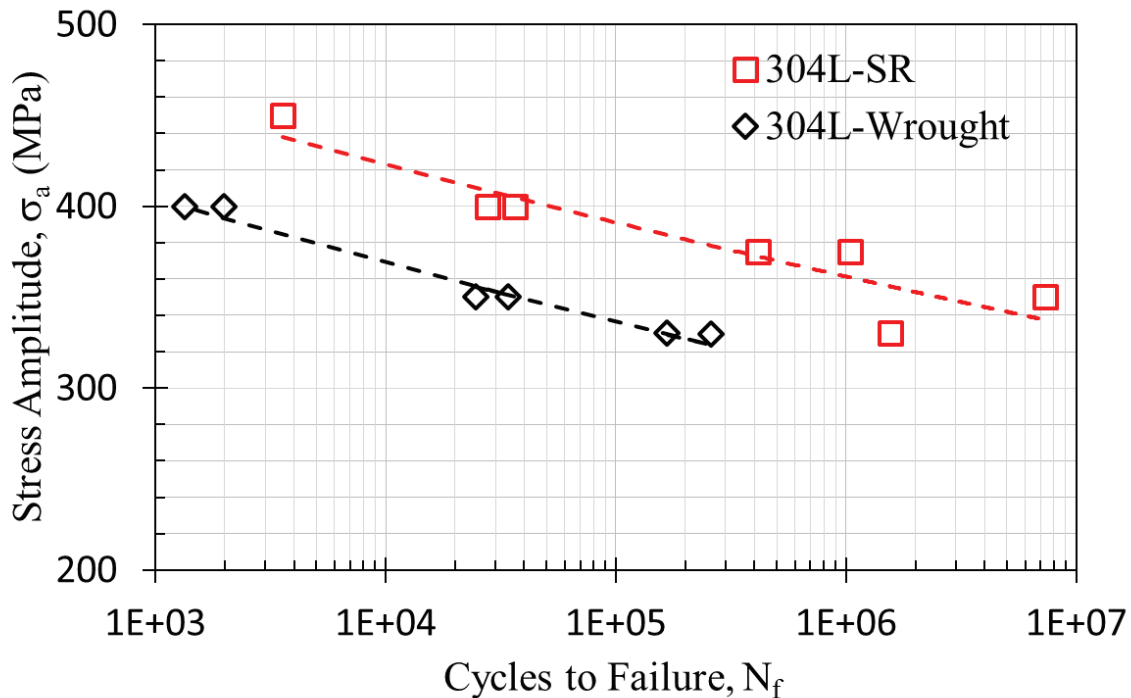


Figure 5: Stress-life fatigue data and related Basquin curves

The ex-situ crack initiation investigation was carried out on the SGF specimens to better understand the failure mechanism associated with the LB-PBF material. Figure 6 shows cracks at 10% of the fatigue life for the stress amplitude of 330 MPa. The 304L-SR specimens showed similar crack lengths at 10% of the HCF life compared to the 304L SS wrought (304L-W) counterpart. Despite the high number of fatigue cycles, the 304L-SR specimens show far less slip activity at the surface as indicated by the persistent slip bands (PSB) in the SEM micro-graphs. Additionally, the 304L-W material shows more developed cracks than the 304L-SR material at a fifth of the fatigue life. Each crack in the 304L-W condition appears to have been deflected by grain boundaries resulting in roughness induced closure and keeping the middle portion of the

crack open. On the other hand, the 304L-SR material shows mostly straight cracks that appear to not have been deflected by neighboring grains.

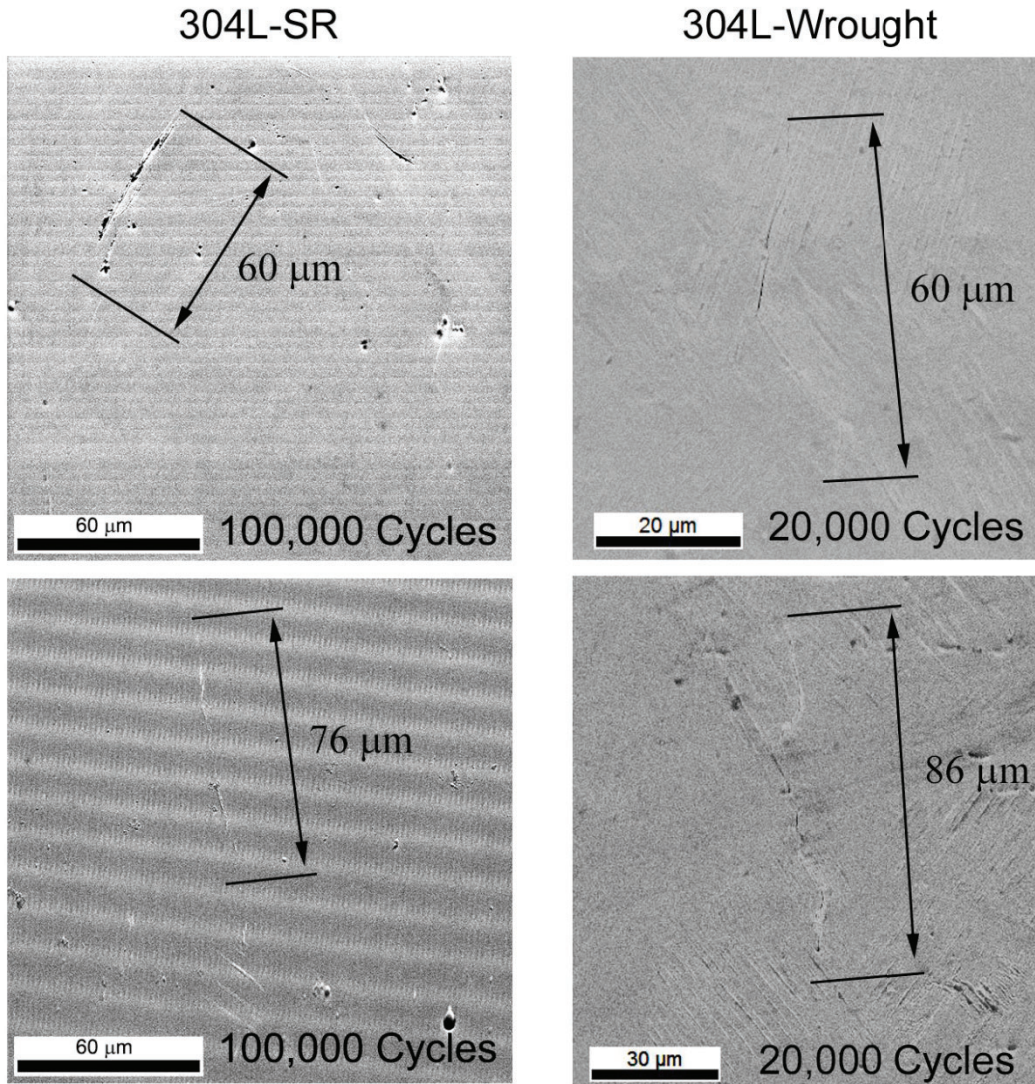


Figure 6: Observed cracks in 304L-SR (left) and 304L-W (right).

The EBSD maps were collected for several cracks to understand mechanisms governing the crack initiation behavior. In order to better understand how the cracks are influenced by the surrounding microstructure, the 304L-SR SGF specimens were cycled further to 300,000 cycles or approximately 30% of the expected fatigue life. Figure 7 shows the IPF map on the left and the Taylor factor map on the right for both 304L-SR cracks shown in Figure 6. Despite being cycled up to 30% of their expected fatigue lives both cracks showed minimal propagation into the surrounding microstructure. This is in stark contrast to the wrought material which after 35,000 cycles had developed a dominant crack approximately 300 μm in length. Unlike the wrought

material where mismatches in Taylor factors across the grain boundary resulted in elastic incompatibilities and crack nucleation [4], the cracks in the 304L-SR material are occurring at grain boundaries with similar Taylor factors. Interestingly, both cracks developed in a region with higher Taylor factors and are bounded by regions of lower Taylor factors.

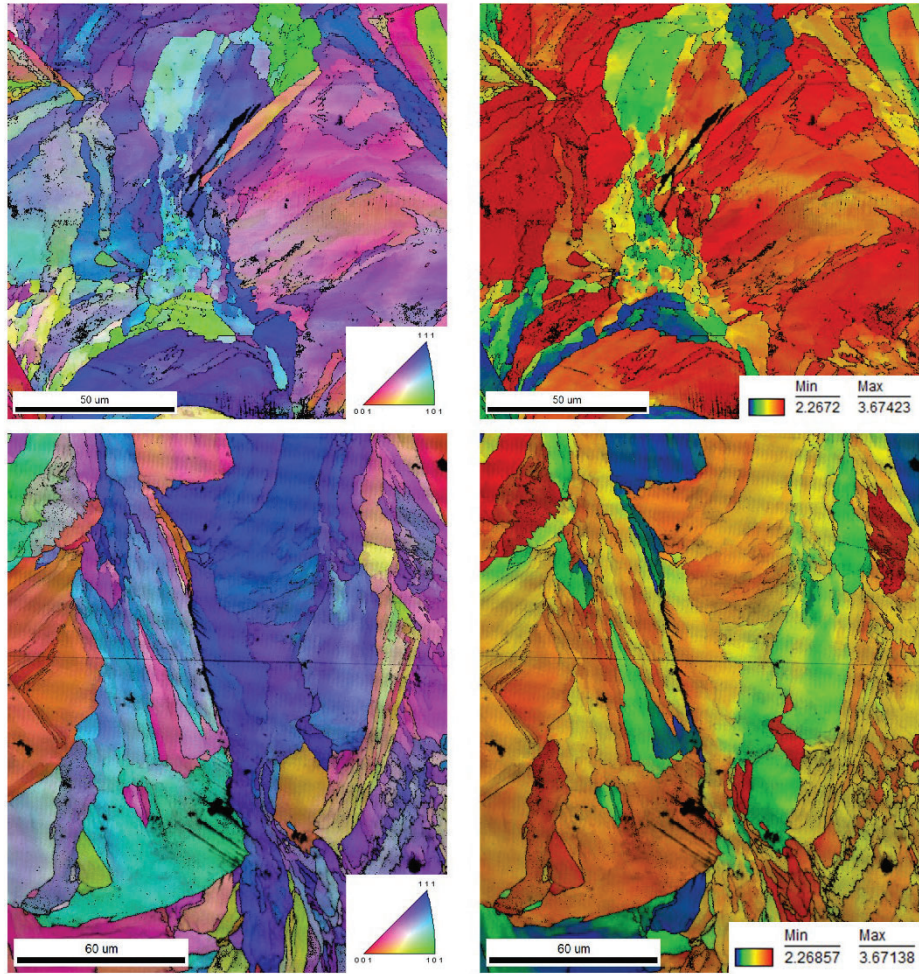


Figure 7: IPF maps (left) and Taylor factor maps (right) for the two 304L-SR cracks shown in Figure 6.

The increase in fatigue strength for LB-PBF 304L SS appears to be attributed to a combination of differences in the as-fabricated microstructure. Most importantly the reduced density of Σ 3-TB and HAGB in the 304L-SR material results in much fewer optimal crack initiation sites for this material. Secondly, the finer microstructure restricts dislocation movement as evident by comparing the 304L-SR and 304L-W SEM images in Figure 6. The wrought material with much larger grains shows a much higher density of PSB on the surface leading to fewer intrusion/extrusions which are also prime crack nucleation features. The PSBs can be observed in relatively large grains with higher Taylor factors, while they are absent from smaller grains that

have low Taylor factors and more efficient slip systems. This indicates that grain size plays a greater role in crack initiation than crystal orientation for 304L-SR.

The effect of grain size on the crack initiation behavior was investigated further using the 304L-SA material which had larger grains as a result of the high temperature annealing procedure. Figure 8 shows the IPF and Taylor factor map of a fatigue crack that has developed in the 304L-SA specimen after only 20,000 cycles. Other than the larger grain size, it can be observed in the Taylor factor map that the crack has occurred at a grain boundary that is approximately 45° from the loading direction and has a significant mismatch in Taylor factor across the HAGB. In fact, all cracks that were observed in the 304L-SA material occurred either at Σ 3-TB/HAGB with mismatched Taylor factors or at discontinuities such as pores on the surface in the vicinity of grains with large Taylor factor mismatches. This observation indicates that the larger grain size results in a shift in the crack initiation mechanism back in line with what is typically observed in 304L-W material.

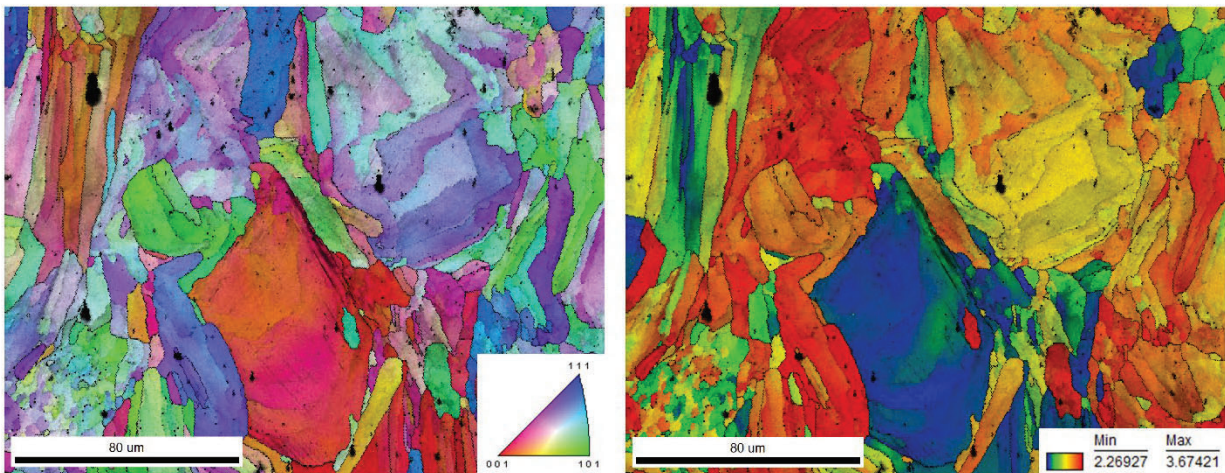


Figure 8: Representative IPF map (left) and Taylor factor map (right) for a crack observed in the 304L-SA conditions.

Conclusions

The aim of this study was to better understand the structure-property relationships of LB-PBF 304L SS. Specifically, the failure mechanisms associated with fatigue crack initiation was investigated through ex-situ experimental EBSD observations of crack initiation and the features resulting in crack initiation. Results indicate that the as-fabricated microstructure in the stress relieved condition has a much higher fatigue strength related to the avoidance of the typical crack initiation mechanisms for wrought 304L SS. The fine microstructure and low Σ 3-TB/HAGB density of the 304L-SR material leads to limited preferred crack initiation sites with cracks forming mainly at HAGB separating grains that are much larger than the average grain size. These cracks propagate until they reach smaller grains after which they slow significantly. This change in crack initiation mechanisms directly leads to the higher strength observed for the 304L-SR condition.

Furthermore, solution annealing the LB-PBF material results in some grain growth with the average grain diameter increasing by approximately 12% from the average diameter of the stress relieved condition. Observations of the crack initiation behavior for the 304L-SA condition showed a shift in the mechanisms back to what is typically observed for wrought 304L SS. Mismatches in Taylor factors along HAGB, leading to elastic incompatibilities and higher localized stress states, were the most frequently observed causes of crack initiation in the 304L-SA material. This resulted in crack formation much earlier in the fatigue life of the 304L-SA condition compared to the 304L-SR material. Thus, by better understanding the feedstock-process-structure-property relationships, additive manufacturing can be used to fabricate net-shaped/near net-shaped parts with improved fatigue resistance.

Acknowledgements

Partial funding for this work was provided by the National Science Foundation under Grant No. 1657195.

References

- [1] N. Shamsaei, A. Yadollahi, L. Bian, S.M. Thompson, An overview of Direct Laser Deposition for additive manufacturing; Part II: Mechanical behavior, process parameter optimization and control, *Additive Manufacturing* 8 (2015) 12-35.
- [2] M. Seifi, M. Gorelik, J. Waller, N. Hrabe, N. Shamsaei, S. Daniewicz, J.J. Lewandowski, Progress towards metal additive manufacturing standardization to support qualification and certification, *Jom* 69(3) (2017) 439-455.
- [3] A. Yadollahi, N. Shamsaei, Additive manufacturing of fatigue resistant materials: Challenges and opportunities, *International Journal of Fatigue* 98 (2017) 14-31.
- [4] J.W. Pegues, M.D. Roach, N. Shamsaei, Influence of microstructure on fatigue crack nucleation and microstructurally short crack growth of an austenitic stainless steel, *Materials Science and Engineering: A* 707 (2017) 657-667.
- [5] M.D. Roach, S.I. Wright, Investigations of twin boundary fatigue cracking in nickel and nitrogen-stabilized cold-worked austenitic stainless steels, *Materials Science and Engineering: A* 607 (2014) 611-620.
- [6] U. Krupp, I. Roth, H.-J. Christ, M. Kübbeler, C.-P. Fritzen, In Situ SEM Observation and Analysis of Martensitic Transformation During Short Fatigue Crack Propagation in Metastable Austenitic Steel, *Advanced Engineering Materials* 12(4) (2010) 255-261.
- [7] A. Heinz, P. Neumann, Crack initiation during high cycle fatigue of an austenitic steel, *Acta Metallurgica et Materialia* 38(10) (1990) 1933-1940.
- [8] P. Neumann, A. Tonnessen, Cyclic deformation and crack initiation, *Fatigue'87* 1 (1987) 3-22.
- [9] M.D. Roach, S.I. Wright, J.E. Lemons, L.D. Zardiackas, An EBSD based comparison of the fatigue crack initiation mechanisms of nickel and nitrogen-stabilized cold-worked austenitic stainless steels, *Materials Science and Engineering: A* 586 (2013) 382-391.

- [10] A. WK49229, New Guide for Orientation and Location Dependence Mechanical Properties for Metal Additive Manufacturing, Book of Standards (2015).
- [11] Z. Sun, X. Tan, S.B. Tor, C.K. Chua, Simultaneously enhanced strength and ductility for 3D-printed stainless steel 316L by selective laser melting, *NPG Asia Materials* 10(4) (2018) 127.
- [12] M.D. Sangid, The physics of fatigue crack initiation, *International Journal of Fatigue* 57 (2013) 58-72.
- [13] A.W. Thompson, W. Backofen, The effect of grain size on fatigue, *Acta metallurgica* 19(7) (1971) 597-606.